Nanoscale

ARTICLE

Supporting Information

Aluminum Nanostructures with Strong Visible-range SERS Activity for Versatile Micropatterning of Molecular Security Labels†

Chee Leng Lay,[a,b] Charlynn Sher Lin Koh,[a] Jing Wang,[c] Yih Hong Lee,[a] Ruibin Jiang,[c] Yijie Yang,[a] Zhe Yang,[a] In Yee Phang,[b] Xing Yi Ling[*,a]

[a.] Division of Chemistry and Biological Chemistry, School of Physical and Mathematical Sciences, Nanyang Technological University, 21 Nanyang Link, Singapore 637371.
Email: xyling@ntu.edu.sg
[b.] Institute of Materials Research and Engineering, Agency for Science, Technology and Research (A*STAR), 2 Fusionopolis Way, Innovis, #08-03, Singapore 138634.
[c.] Shaanxi Engineering Lab for Advanced Energy Technology, School of Materials Science and Engineering, Shaanxi Normal University, Xi'an, China 710119.

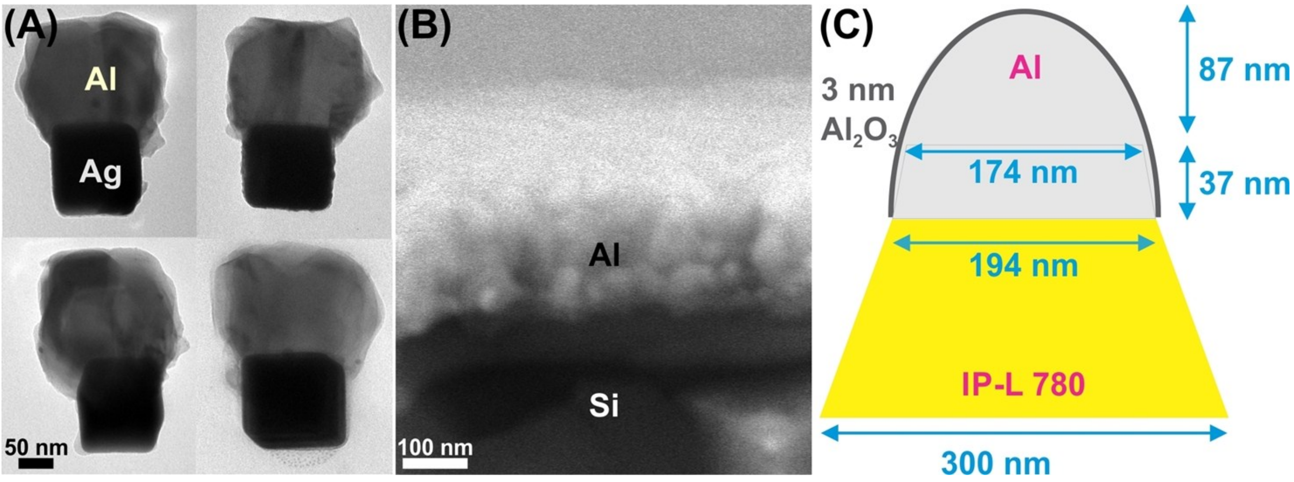

Fig. S1 (A) TEM micrographs of Al layers deposited on silver nanocubes (edge-to-edge length (120 ± 10 nm)). The TEM micrograph displays depositing morphology of the Al layers on nanostructures with similar width as the silver nanocubes, facilitating model design for FDTD simulations on the Al-deposited IP-L 780 polymeric nanostructures. (B) SEM cross-sectional view of Al layer coated on a silicon wafer. Average thickness of the Al layer is (115 ± 8) nm. (C) Model of Al-coated IP-L 780 nanostructure used for FDTD simulations.

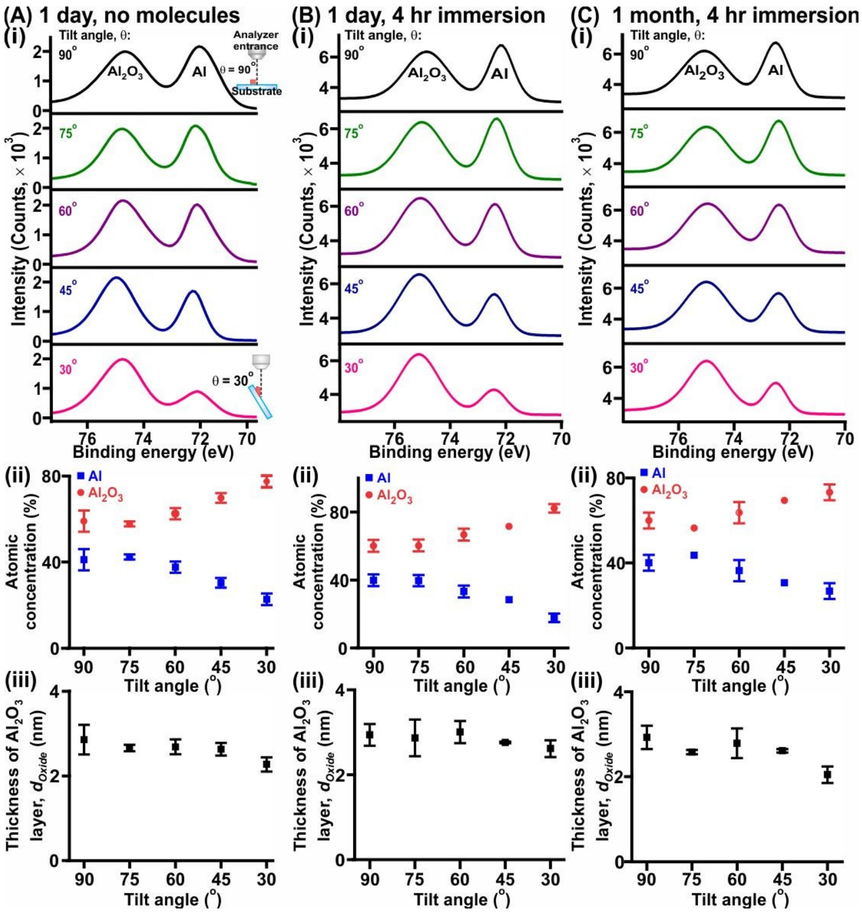

Fig. S2 We investigate the stability of Al_2O_3 layer on Al-coated substrates (A) 1 day after Al deposition, (B) 1 day after Al deposition and 4 hour after immersion in TEPS ethanolic solution, and (C) 1 month after Al deposition and 4 hour after immersion in TEPS ethanolic solution. (i) Dependence of XPS spectra on tilt angle for 100-nm thin Al film which was evaporated under the same conditions as in fabrication of Al nanostructures. (Inset) Schematic depiction on tilt angle, defined as the angle between the plane of the sample surface and the entrance to the analyzer. The low energy (~ 72.9 eV) and high energy (~ 74.4 eV) shoulders correspond to the Al 2p line from Al and Al_2O_3, respectively. (ii) Calculated elemental distribution of Al and Al_2O_3 as a function of tilt angle based on angle dependence of ratio between the area under the curves of the Al metal peak and Al 2p oxide peak. (iii) Calculated thickness of Al_2O_3 layer against tilt angles.

Using angle-resolved X-ray photoelectron spectroscopy (XPS), we quantify the thickness of aluminum oxide (Al_2O_3) on our Al nanostructures by varying the angle between the detector and the Al samples from 90 ^{o} to 30 ^{o} (Fig. 1C, Fig. S2). It is observed that Al_2O_3 content increases as more near-surface compositions are measured at lower tilt angles (Fig. 1C(i)), verifying formation of very thin Al_2O_3 layer at the surface of Al samples. The thickness of the homogenous native oxide layer after 24 h of exposure to ambient conditions (25 °C, 65% relative humidity) is approximately 3 nm (Fig. S2, Equation S1). The 3-nm thick oxide layer is fairly dense and stable in preventing oxygen diffusion which dramatically slows down the oxidation process.[1, 2] After keeping in nitrogen box for a month, the Al nanodots remain stable and provide consistent SERS performance after molecular adsorption (Fig. 2D, Fig. S2). Moreover, Raman peak recorded at 1330 cm^{-1} for NAP adsorbed Al nanodots after 1-month storage only experiences less than 30 % drop in SERS intensity (Fig. 2D). Consequently, the stable SERS signals imply that the oxide layer is sufficiently dense to prevent oxygen diffusion towards the Al core, in turn dramatically slowing down the corrosion of the Al nanodots to preserve the SERS-activity of our platform.[1, 2]

Characterization of the aluminum oxide layer using XPS

Thickness of aluminum oxide layer is calculated using Equation S1:[3]

$$d_{Oxide} = \lambda_{Oxide} sin\theta ln\left(\frac{\rho_{Al}\lambda_{Al}A_{Oxide}}{\rho_{Oxide}\lambda_{Oxide}A_{Al}} + 1\right) \qquad \text{------ Equation S1}$$

ρ_{Al} = Volume density of aluminum = 0.1 mol/cm^{-3}

ρ_{Oxide} = Volume density of aluminum oxide = 0.0777 mol/cm^{-3}

λ_{Al} = Inelastic mean free path of electrons in aluminum = 2.8 nm

λ_{Oxide} = Inelastic mean free path of electrons in aluminum oxide = 2.6 nm

A_{Al} and A_{Oxide} = Area under the curve of fit curves to the experimental results

θ = Tilt angle of the substrate with respect to the XPS detector. This angle corresponds to the take-off angle of photoelectrons from the substrate’s surface.

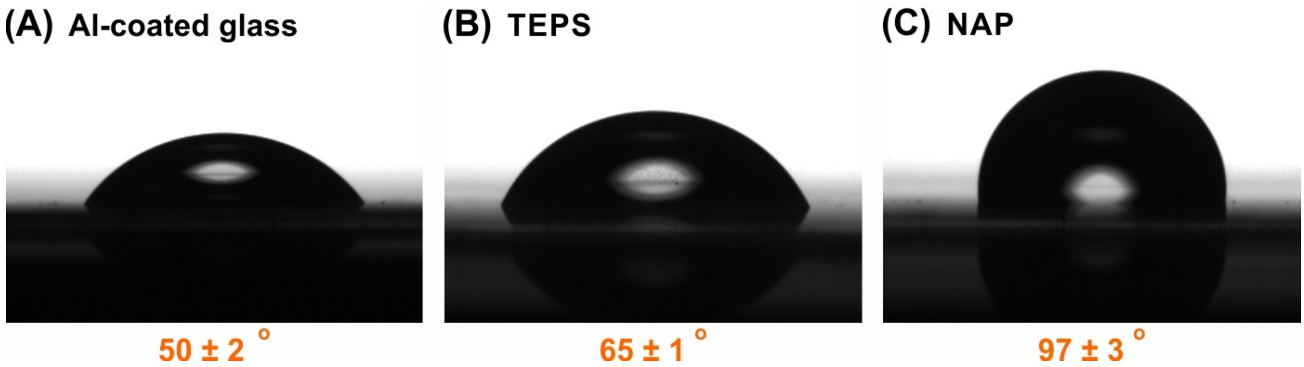

Fig. S3 Water contact angle measurements for (A) Al-coated glass substrate, (B) TEPS- and (C) NAP-adsorbed Al-coated substrate.

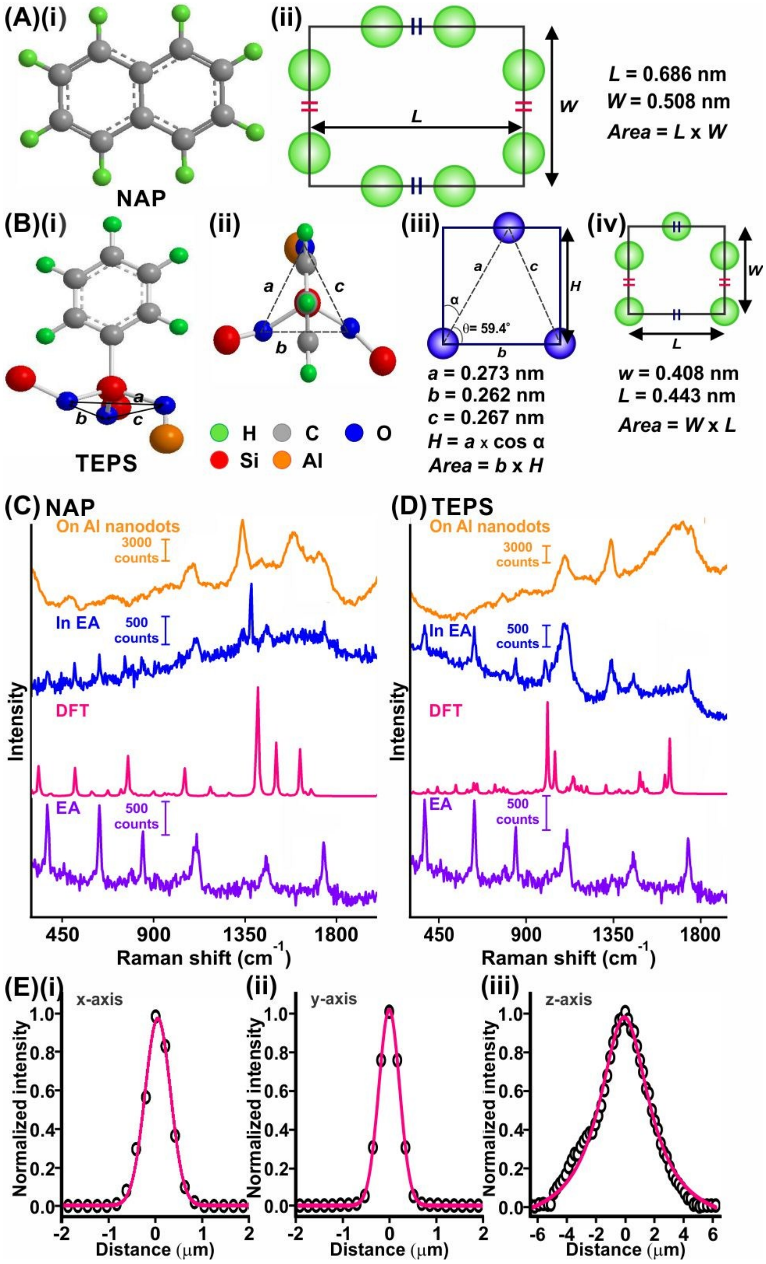

Fig. S4 (A)(i) top view of DFT-simulated structural configuration of NAP molecules, and (ii) geometry calculation on theoretical molecular occupying area of NAP molecules on Al. (B)(i) Side view and (ii) top view of simulated structural configuration of TEPS molecules, respectively. Geometry calculation on theoretical molecular occupying area of TEPS molecules on Al based on (iii) distance between O atoms and (iv) size of phenyl ring on TEPS, respectively. (C) SERS spectrum of NAP molecules adsorbed on Al-coated IP-L 780 nanodots (orange), normal Raman spectrum of 1 M NAP in ethyl acetate (blue), DFT simulated graph for NAP (pink) and normal Raman spectrum of ethyl acetate (violet). (D) SERS spectrum of TEPS molecules adsorbed on Al-coated IP-L 780 nanodots (orange), normal Raman spectrum of 1 M TEPS in ethyl acetate (blue), DFT simulated graph for TEPS (pink) and normal Raman spectrum of ethanol (violet). Intensity at ~ 1330 cm^{-1} Raman band from both molecules is used for calculating SERS EF. (E) Optical resolutions of 532 nm laser passing through Nikon TU Plan ELWD 100x objective lens (NA 0.8) for (i) x-, (ii) y- and (iii) z-axis, respectively.

The simulated distance between H atoms for phenyl rings and O atoms on the probe molecules are listed in Fig. S4A and S4B. From calculations, the theoretical molecular occupying area of a NAP molecule on Al is 0.348 nm^2 (Fig. S4A(ii)). On the other hand, the estimated molecular area of a TEPS molecule based on O atoms on silane is 0.062 nm^2 (Fig. S4B(iii)) and the area becomes 0.181 nm^2 when phenyl group (Fig. S4B(iv)) is considered. Our calculated molecular areas of NAP and TEPS molecule are much smaller than the reported molecular areas of NAP and benzene, which are 0.65 nm^2, and 0.30 to 0.43 nm^2, respectively.[4-6] Therefore, our calculated molecular areas assume the closest packing of probe molecules on the Al surfaces. The estimated SERS EFs are thus underestimated.

We observe that the experimental Raman peaks of NAP at 1090 cm^{-1}, 1330 cm^{-1} and 1590 cm^{-1} are respectively shifted to 1055 cm^{-1}, 1411 cm^{-1} and 1624 cm^{-1} in the simulated results (Fig. S4C). On the other hand, Raman peaks of TEPS at 1090 cm^{-1}, 1330 cm^{-1} and 1700 cm^{-1} are shifted to 1050 cm^{-1}, 1310 cm^{-1} and 1642 cm^{-1} respectively in the simulated results (Fig. S4D). The main reason for the blue/red shift in the Raman peaks is the difference in structure between the compact passivating Al_2O_3 layer and the simulated Al_2O_3-molecules model. Moreover, the DFT simulation with single molecule neglects the neighbouring effects of close-packed molecules grafted on surface which deviate the experimental SERS bands.[7, 8] Nevertheless, the presence of aforementioned Raman characteristic peaks provides strong evidence on the adsorption of NAP and TEPS molecules onto Al surfaces.

Calculation of SERS enhancement factor

To calculate SERS enhancement factor (EF) of the fabricated Al-coated IP-L 780 nanostructures, Equation S2 is used. To simplify SERS EF calculation, Al-coated IP-L 780 nanodots with diameter of (196 ± 20) nm and thickness of (115 ± 8) nm are used for SERS measurements. Both SERS and normal Raman measurements are conducted using point mode with laser power of 40 mW and exposure time of 20 s. By using Equation S2 and the theoretical molecular occupying area of a NAP or a TEPS molecule, it is assumed that a monolayer of NAP or TEPS molecules with the closest molecular packing is adsorbed on surfaces of the Al-coated IP-L 780 nanostructures.

$$EF = \frac{I_{SERS}}{N_{SERS}} / \frac{I_{Normal}}{N_{Normal}}$$

------Equation S2

(A) NAP

I_{SERS} = Intensity of the 1330 cm^{-1} Raman band from NAP adsorbed on Al-coated IP-L 780 microstructures

= 7656 counts

N_{SERS} = Number of NAP molecules contributing to I_{SERS}

= Surface area of the deposited Al film / molecular occupying area of a NAP molecule

The deposited Al film on IP-L 780 micro-dot is assumed as a hemisphere, so

Surface area = $2\pi r^2$

= 60344 nm^2

Therefore,

N_{SERS} = 60344 / 0.348

= 173402 molecules

I_{Normal} = Intensity of the 1330 cm^{-1} Raman band from 1 M NAP – ethyl acetate solution (same laser power and acquisition time as for I_{SERS} measurements)

= 1134 counts

N_{Normal} = Number of NAP molecules that yield I_{Normal}.

= Volume of laser spot × Concentration of NAP × Avogadro’s number

To determine volume of laser spot, the lateral spot size of the focus beam is measured from the displayed laser spot that gives the highest sample signal. The axial size of the laser is determined by adjusting the stage position along the z-axis (optical path) to get the z-distance from maximum signal intensity to zero intensity. The lateral and axial spot sizes are used to get optical resolutions of the 532 nm laser, which are: x = (914 ± 110) nm; y = (850 ± 55) nm; and z = (4880 ± 247) nm. And,

Volume of laser spot = $[\pi \times (x / 2) \times (y / 2) \times z] / 10^{21}$

= 2.978×10^{-12} cm^3

Therefore,

N_{Normal} $= 2.978 \times 10^{-12} \times 1 \times 6.023 \times 10^{23} \times 0.001$
$= 1.794 \times 10^{9}$ molecules

SERS EF $= (7656 / 173402) / (1134 / 1.794 \times 10^{9})$
$= 7.0 \times 10^{4}$

<u>(B)</u> <u>TEPS</u>

I_{SERS} = Intensity of the 1330 cm^{-1} Raman band from TEPS adsorbed on aluminum-coated IP-L 780 microstructures
= 7163 counts

The theoretical molecular occupying area of a TEPS molecule on aluminum is 0.062 nm^{2}, so

N_{SERS} = Number of TEPS molecules contributing to I_{SERS}
= 60344 / 0.062
= 973290 molecules

I_{Normal} = Intensity of the 1330 cm^{-1} Raman band from 1 M TEPS – ethyl acetate solution
= 779.65 counts

N_{Normal} = Number of TEPS molecules that yield I_{Normal}
$= 2.978 \times 10^{-12} \times 1 \times 6.023 \times 10^{23} \times 0.001$
$= 1.794 \times 10^{9}$ molecules

SERS EF $= (7163.39 / 973290) / (779.65 / 1.794 \times 10^{9})$
$= 1.7 \times 10^{4}$

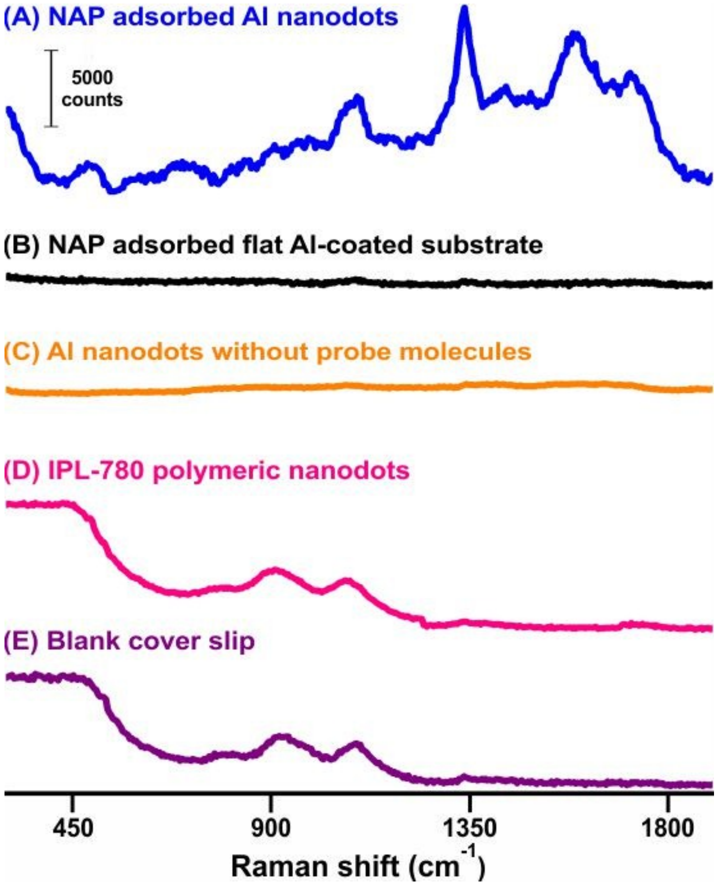

Fig. S5 Comparison of SERS intensity of (A) NAP adsorbed Al nanodots, (B) NAP adsorbed flat Al-coated glass substrate, (C) Al nanodots without probe molecules, (D) IP-L 780 polymeric nanodots and (E) blank cover slip only. As observed, there is no interference from background signals on SERS intensity of NAP adsorbed Al nanodots.

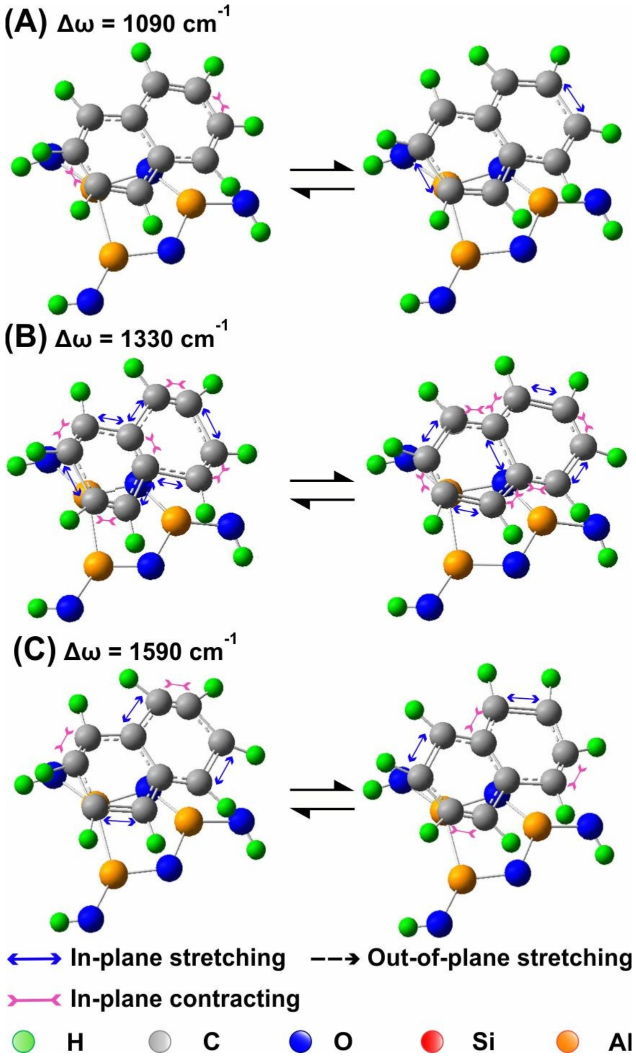

Fig. S6 Schematic representatives for DFT-simulated vibrational modes of the NAP molecules adsorbed on Al surfaces at Raman shift (A) 1090 cm^{-1}, (B) 1330 cm^{-1} and (C) 1590 cm^{-1}.

To understand types of vibration in TEPS molecules adsorbed on Al surfaces upon 532-nm excitation, we capture the molecular vibration animations obtained from the DFT simulation at Raman shifts of (A) 1090 cm^{-1}, (B) 1330 cm^{-1} and (C) 1590 cm^{-1}. These three Raman peak positions are the dominant peaks observed from our measured SERS spectra (Fig. 2C and Fig. S4C). Fig. S6 illustrates that vibrations of the phenyl rings on the TEPS molecules give raise to the major SERS signals. The peak at 1090 cm^{-1} represents the phenyl ring CCC symmetric stretching vibration mode. On the other hand, the peaks at 1330 cm^{-1} and 1590 cm^{-1} represent the in-plane phenyl ring asymmetric stretching mode.[9, 10] The presence of aforementioned vibrational modes provides strong evidence on the physisorption of NAP molecules onto Al surfaces.

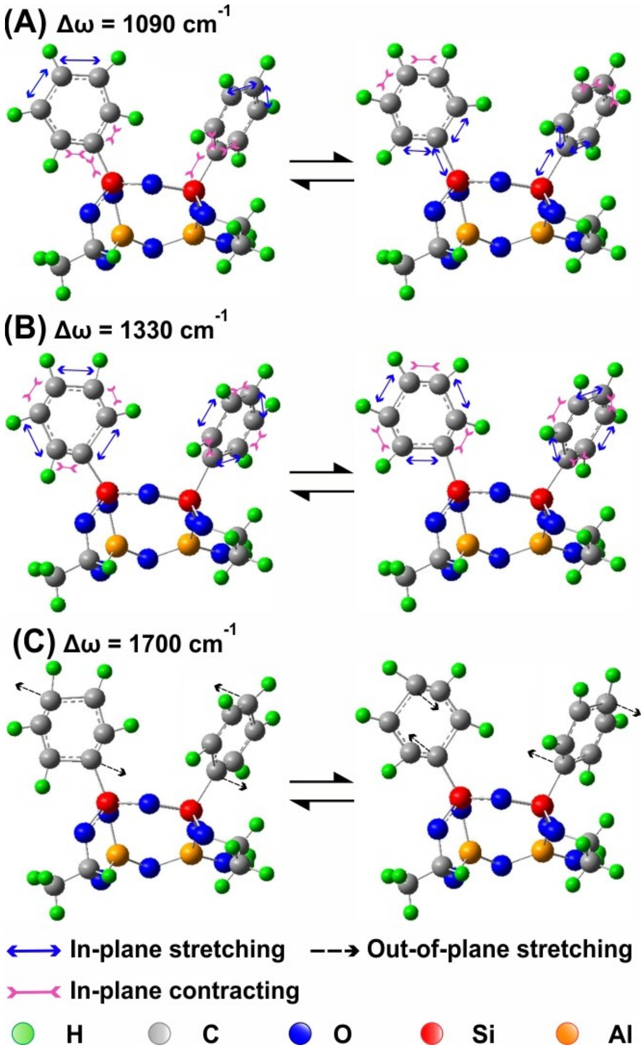

Fig. S7 Schematic representatives for DFT-simulated vibrational modes of the TEPS molecules adsorbed on Al surfaces at Raman shift (A) 1090 cm^{-1}, (B) 1330 cm^{-1} and (C) 1700 cm^{-1}.

To understand types of vibration in TEPS molecules adsorbed on Al surfaces upon 532-nm excitation, we capture molecular vibrations animations displayed in DFT simulation at Raman shifts of (A) 1090 cm^{-1}, (B) 1330 cm^{-1} and (C) 1700 cm^{-1}. These three Raman peak positions are the dominant peaks observed from our measured SERS spectra (Fig. 2C and Fig. S4D). Fig. S7 illustrates that vibrations of the phenyl rings on the TEPS molecules give raise to the major SERS signals. From the simulation, the peak at 1090 cm^{-1} represents the phenyl ring CCC symmetric stretching vibration mode. On the other hand, the peak at 1330 cm^{-1} is due to the in-plane phenyl ring asymmetric stretching mode, while out-of-plane phenyl-ring stretching mode is observed at peak 1700 cm^{-1}.[9, 10] The presence of aforementioned vibrational modes provides strong evidence on the chemisorption of TEPS molecules onto Al surfaces.

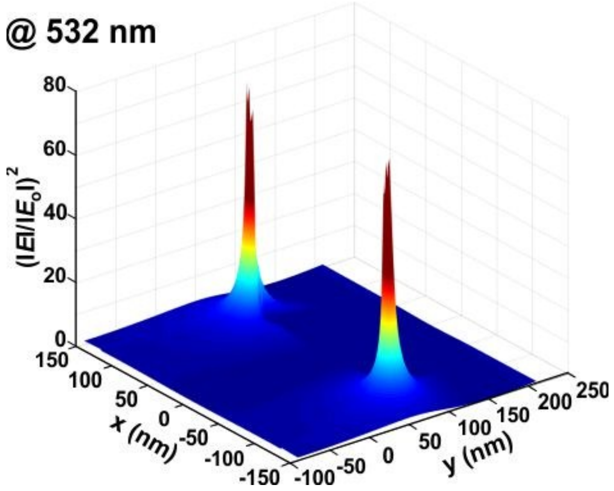

Fig. S8 Electric field intensity ($|E|/|E_o|)^2$ of an Al nanodot simulated at excitation wavelength of 532 nm.

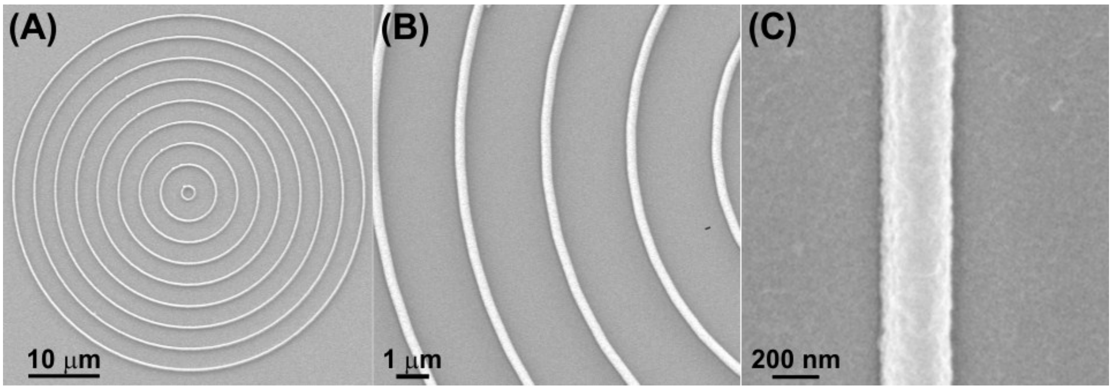

Fig. S9 SEM micrographs of concentric ring structure consisting of continuous Al nanowires at different magnifications.

The width and periodicity of the Al nanowires are set at (170 ± 20) nm and 2 μm to minimize plasmonic coupling between neighboring nanowires (Fig. 3A, Fig. S9).[11]

References

1. G. H. Chan, J. Zhao, G. C. Schatz and R. P. Van Duyne, *J. Phys. Chem. C*, 2008, **112**, 13958-13963.
2. W. M. Haynes, *CRC Handbook of Chemistry and Physics, 95th Edition*, CRC Press, 2014.
3. S. Ayas, A. E. Topal, A. Cupallari, H. Güner, G. Bakan and A. Dana, *ACS Photonics*, 2014, **1**, 1313-1321.
4. K. K. Qian, S. L. Suib and R. H. Bogner, *J. Pharm. Sci.*, 2011, **100**, 4674-4686.
5. A. L. McClellan and H. F. Harnsberger, *J. Colloid. Interface Sci.*, 1967, **23**, 577-599.
6. A. Nonaka, *Colloids Surf.*, 1992, **62**, 207-213.
7. L. Laurentius, S. R. Stoyanov, S. Gusarov, A. Kovalenko, R. Du, G. P. Lopinski and M. T. McDermott, *ACS Nano*, 2011, **5**, 4219-4227.
8. X. Han, H. K. Lee, Y. H. Lee, W. Hao, Y. Liu, I. Y. Phang, S. Li and X. Y. Ling, *J. Phys. Chem. Lett.*, 2016, **7**, 1501-1506.
9. T. Shimanouchi, *J. Phys. Chem. Ref. Data*, 1972, **1**, 189-216.
10. D. W. Mayo, in *Course Notes on the Interpretation of Infrared and Raman Spectra*, John Wiley & Sons, Inc., 2004, DOI: 10.1002/0471690082.ch5, pp. 101-140.
11. Y. Cui, I. Y. Phang, R. S. Hegde, Y. H. Lee and X. Y. Ling, *ACS Photonics*, 2014, **1**, 631-637.